# Histological assessments for toxicity and functionalization-dependent biodistribution of carbon nanohorns

**Article** *in* Nanotechnology · July 2011

DOI: 10.1088/0957-4484/22/26/265106 · Source: PubMed

CITATIONS
33

READS
52

**8 authors**, including:

Yoshio Tahara
National Institute of Advanced Industrial Science and Technology
**12** PUBLICATIONS **685** CITATIONS
SEE PROFILE

Jin Miyawaki
Kyushu University
**162** PUBLICATIONS **3,447** CITATIONS
SEE PROFILE

Minfang Zhang
National Institute of Advanced Industrial Science and Technology
**96** PUBLICATIONS **1,931** CITATIONS
SEE PROFILE

Mei Yang
National Institute of Advanced Industrial Science and Technology
**18** PUBLICATIONS **243** CITATIONS
SEE PROFILE

Histological assessments for toxicity and functionalization-dependent biodistribution of carbon nanohorns



2011 Nanotechnology 22 265106

(http://iopscience.iop.org/0957-4484/22/26/265106)

Nanotechnology **22** (2011) 265106 (8pp) doi:10.1088/0957-4484/22/26/265106

# Histological assessments for toxicity and functionalization-dependent biodistribution of carbon nanohorns

**Yoshio Tahara**[1], **Jin Miyawaki**[2,7], **Minfang Zhang**[1,2], **Mei Yang**[1,5], **Iwao Waga**[3], **Sumio Iijima**[1,2,4,5], **Hiroshi Irie**[6] and **Masako Yudasaka**[1,2,7]

[1] Nanotube Research Center, National Institute of Advanced Industrial Science and Technology, 5-2, 1-1-1 Higashi, Tsukuba, Ibaraki 305-8565, Japan
[2] JST/SORST, c/o NEC, 34 Miyukigaoka, Tsukuba, Ibaraki 305-8501, Japan
[3] VALWAY Technology Center, NEC Soft, Ltd, 1-18-7, Shinkiba, Koto-Ku, Tokyo 136-8627, Japan
[4] NEC, 34 Miyukigaoka, Tsukuba, Ibaraki 305-8501, Japan
[5] Department of Material Science and Engineering, Meijo University, 1-501 Shiogamaguchi, Tenpaku, Nagoya 468-8502, Japan
[6] Teikyo University School of Medicine, 2-11-1 Kaga, Itabashi-ku, Tokyo 173-8605, Japan

E-mail: miyawaki@cm.kyushu-u.ac.jp and m-yudasaka@aist.go.jp

Received 14 January 2011, in final form 7 April 2011
Published 18 May 2011
Online at stacks.iop.org/Nano/22/265106

**Abstract**
Single-walled carbon nanohorns (SWNHs) intravenously administered to mice did not show severe toxicity during a 26-week test period, which was confirmed by normal gross appearance, normal weight gain and the lack of abnormality in the tissues on histological observations of the mice. SWNH biodistribution was influenced by chemical functionalization. Accumulation of SWNH in the lungs reduced as SWNH hydrophilicity increased; however, the most hydrophilic SWNHs modified with bovine serum albumin (BSA) were most likely to be trapped in the lungs, suggesting that the BSA moiety enhanced macrophage phagocytosis in the lungs. Clearance of some of the hydrophobic SWNHs from the lungs was observed, the mechanism of which is briefly discussed.

S Online supplementary data available from stacks.iop.org/Nano/22/265106/mmedia

(Some figures in this article are in colour only in the electronic version)

## 1. Introduction

Carbon nanotubes [1, 2] are attractive candidates for various biomedical applications such as drug delivery [3–5]. Their toxicity and biodistribution depends on the size, shape, agglomeration and chemical functionalization of the molecules [6–9]. Recent reports suggest that long, rigid rod-like multi-walled carbon nanotubes (MWNTs) cause toxic lesions and inflammation because they are not completely engulfed by macrophages due to their length, which results in phagocytotic frustration and leads to the generation of toxic materials such as reactive oxygen species [7, 10]. On the other hand, short MWNTs engulfed by macrophages do not induce phagocytotic frustration [11]. Similar to MWCNTs, the toxicity of single-walled carbon nanotubes (SWNTs) depends on their length and aggregation states [8, 9].

Biodistribution studies have revealed that MWNTs and SWNTs are usually captured by macrophages and accumulated in the lungs, liver, spleen and other reticuloendothelial systems [12], suggesting the need for long-term toxicity studies. On the other hand, depending on their length, diameter and chemical functionalization, they are excreted out of the living body [13, 14].

To establish the relationship of toxicity and biodistribution of nanocarbons with size, shape, agglomeration and functionalization, toxicity and biodistribution with regard to

[7] Authors to whom any correspondence should be addressed.

 

various types of nanocarbons should be studied. Therefore, we studied the toxicity and biodistribution of single-walled carbon nanohorns (SWNHs). SWNHs are single graphene tubules with diameters of 2–5 nm and lengths of 40–50 nm. Approximately 2000 SWNHs assembled to form a robust spherical aggregate with a diameter of approximately 100 nm [15]. Since SWNHs do not contain metals, their toxicity and biodistribution can be discussed without considering the effects of metals. We previously confirmed that *in vivo* acute toxicity (dermatoxicity, mutagenicity test, peroral toxicity and others) for pristine SWNHs was low [16]. In this study, we discuss how chemical functionalization influences SWNH toxicity and biodistribution when administered intravenously. We used three types of functionalized nanohorns (figure 1): (1) hydrophobic oxSWNH obtained by slow combustion in air [17], (2) hydrophilic light-assisted $H_2O_2$ oxidation (LAOx)-SWNH obtained by LAOx [18] and (3) BSA–LAOx-SWNH prepared from LAOx-SWNH by chemical functionalization with bovine serum albumin (BSA). LAOx-SWNHs have higher numbers of oxygen-containing functional groups, such as carboxyl groups, at the hole edges than oxSWNHs [18]. BSA–LAOx-SWNHs disperse well in phosphate buffered saline (PBS) and can be taken up by mammalian cells [18].

## 2. Experimental section

### *2.1. Sample preparation*

SWNHs were prepared by $CO_2$ laser ablation of a pure graphite target containing no metal catalyst in an Ne atmosphere (760 Torr) at room temperature [15]. SWNHs were then heated at 1200 °C for 3 h under an $H_2$ flow (300 ml $min^{-1}$, 760 Torr) to remove amorphous carbon. The holes of the $H_2$-treated SWNHs were opened by slow combustion or LAOx methods. In the slow combustion method [17], the $H_2$-treated SWNHs were heated up to 550 °C at a ramping rate of 1 °C $min^{-1}$ under a dry air flow followed by natural cooling to room temperature (oxSWNHs). In the LAOx method [18], 50 mg of the $H_2$-treated SWNHs were dispersed in 50 ml of 30% $H_2O_2$ and stirred on a hot plate at 100 °C under light irradiation ($\lambda = 250$–2000 nm, 3 W) for 2 h. After filtration with a 0.2 $\mu$m membrane filter and rinsing with ultrapure water twice, half of the black material on the filter was dispersed in ultrapure water and dried in air at 70 °C (LAOx-SWNHs). The other half was dispersed in 25 ml of PBS (pH 7.4) and used for reaction with BSA. For chemical modification with BSA [17], carboxylic groups of LAOx-SWNHs were activated by sonication with 220 mg of 1-ethyl-3-[3-(dimethylamino)propyl]carbodiimide (EDAC, Sigma-Aldrich) for 2 h. Then 500 mg of BSA (Sigma-Aldrich, 66 kDa) was added to the slurry and sonication was continued for another 20 min, followed by stirring for 24 h at room temperature. After repeated filtration/rinsing three times to remove unreacted EDAC and BSA, the black material on the filter was dispersed in ultrapure water and lyophilized. The final product was designated as BSA–LAOx-SWNHs.

### *2.2. Sample characterization*

The structure of nanohorn samples was observed under a transmission electron microscope (TEM; Topcon Co., EM-002B) at an acceleration voltage of 120 kV. The quantity of covalently bonded BSA was roughly estimated by thermogravimetric analysis (TGA; TA instruments, TGA2950) in $O_2$ as the weight-loss difference at 400 °C between samples before and after BSA attachment. Total pore volume was estimated from the thermal desorption quantity of m-xylene ($W_{xylene}$) measured by TGA in He [16, 17]. Briefly, m-xylene was pre-adsorbed on SWNHs by exposure to saturated vapors of m-xylene in a closed container for 1 h at room temperature. TGA measurements were performed after specimens were placed in the TGA apparatus under an He gas flow (100 ml $min^{-1}$) for 30 min. $W_{xylene}$ was estimated from the weight-loss difference at 300 °C between samples with and without m-xylene adsorption. To estimate pore volume, a calibration curve between $W_{xylene}$ and the pore volume obtained from $N_2$ adsorption isotherm measurements at 77 K [17] (supporting information I available at stacks.iop.org/Nano/22/265106/mmedia) was used.

Particle size distributions in the nanohorn-PBS dispersions were estimated by the dynamic light scattering method (DLS; Otsuka Electronics Co. Ltd, FPAR-1000). Their $\zeta$ potentials were measured using a laser $\zeta$-electrometer (Otsuka Electronics Co. Ltd, ELS-6000). In $\zeta$-potential measurements, an aliquot (0.1 ml) of the administered solution was diluted with 15 ml of ultrapure water.

### *2.3. Animal tests*

The animal experiments were performed at Toray Research Center, Inc. Under the specific-pathogen-free condition, 20 male mice (Slc:ICR, 8 weeks old upon arrival) obtained from Japan SLC Inc.were housed individually in plastic cages under controlled laboratory conditions (19–25 °C, 40–60% relative humidity, 12 h/12 h light/dark cycle). They were allowed free access to standard pellets (CRF-1, Oriental Yeast Co., Ltd) and ultraviolet-disinfected drinking water. The animals were acclimated to this environment for 1 week before SWNH administration. At the time of administration (day 0), they were 9 weeks old and weighed 35.0–44.0 g. The animals were treated according to the Institutional Animal Care and Use Guidelines.

We independently performed single-dose intravenous administration tests for oxSWNHs (test 1) and for LAOx-SWNHs and BSA–LAOx-SWNHs (test 2). Each test contained respective control groups in which animals were given a single injection of Dulbecco's PBS (Wako Pure Chemical Industries, Ltd) at a dosage of 8 ml $kg^{-1}$ of body weight. Three observation periods of 2, 4 and 26 weeks (2 w, 4 w and 26 w) were set. Each group contained five mice. To prepare test samples, nanohorn samples were suspended in PBS and sonicated using an ultrasonic bath for about 10 min for homogeneous dispersion. Concentrations were set at 0.75 mg $ml^{-1}$ for oxSWNHs and LAOx-SWNHs and 1.0 m $ml^{-1}$ for BSA–LAOx-SWNHs (LAOx-SWNH: 0.75 mg $ml^{-1}$). The suspensions were further vortexed and immediately injected in the tail vein using a 1 ml disposable syringe barrel with a 26 or 27 G needle at a dosage of 8 ml $kg^{-1}$ of body weight (6 mg $kg^{-1}$ of body weight for oxSWNHs and

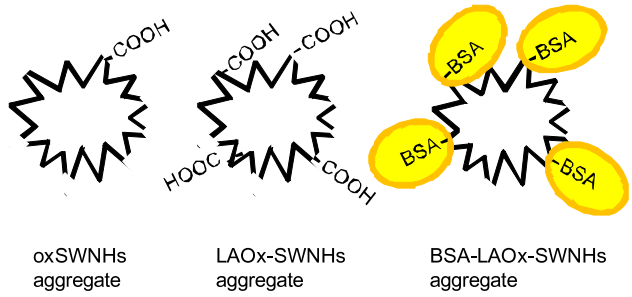


**Figure 1.** Schematic illustration of oxSWNH, LAOx-SWNH and BSA–LAOx-SWNH agglomerates.

LAOx-SWNHs or 8 mg $kg^{-1}$ of body weight for BSA–LAOx-SWNHs).

After the test periods, animals were euthanized by exsanguination under pentobarbital anesthesia, and their organs and tissues were autopsied. Organs (brain, heart, lungs, liver, kidneys and spleen) were fixed in 10% buffered formalin, embedded in paraffin, sectioned, stained with hematoxylin and eosin (HE), and then histopathologically observed under an optical microscope. Body weight was measured on days 0, 1, 3, 4, 7, 11 and 14, and once a week thereafter. The Mitsui Toxicological Data Processing System (protocol no. 05T053) was used for animal grouping, which grouped animals according to body weight after acclimation, and data collection of clinical signs, mortality, gross autopsy findings, histopathological findings and body weights.

### *2.4. Immunohistochemistry*

Immunohistochemical staining of macrophages was performed at Hist Science Laboratory Co., Ltd. In brief, 4 $\mu$m sections were prepared from the paraffin blocks. The sections were deparaffinized in xylene and ethanol. After rinsing, endogenous peroxidase was blocked by incubation with 3% $H_2O_2$ for 5 min. The sections were then incubated overnight with rat anti-mouse LAMP-2 (CD107b) antibody (M3/84) (1:25) (Santa Cruz Biotechnology) at 4 °C. Following rinsing, they were incubated with the secondary antibody, Histofine Simple Stain Mouse MAX PO (Rat) (Nichirei), for 30 min at room temperature. After washing, CD107b-specific immunolabeling was examined using diaminobenzidine (Nichirei). In addition, nuclei were stained with hematoxylin.

## 3. Results

### *3.1. Sample characterization*

TEM images show that oxSWNHs (figure 2(a)), LAOx-SWNHs (figure 2(c)) and BSA–LAOx-SWNHs (figure 2(e)) maintained the spherical aggregate forms of as-grown SWNHs. The holes opened at the tips, and sidewalls of oxSWNHs and LAOx-SWNHs were visible in their TEM images (arrows in figures 2(b) and (d)). BSA molecules in BSA–LAOx-SWNHs, most likely damaged by electron beams, appeared to be attached to agglomerate surfaces (figure 2(f)) [18].

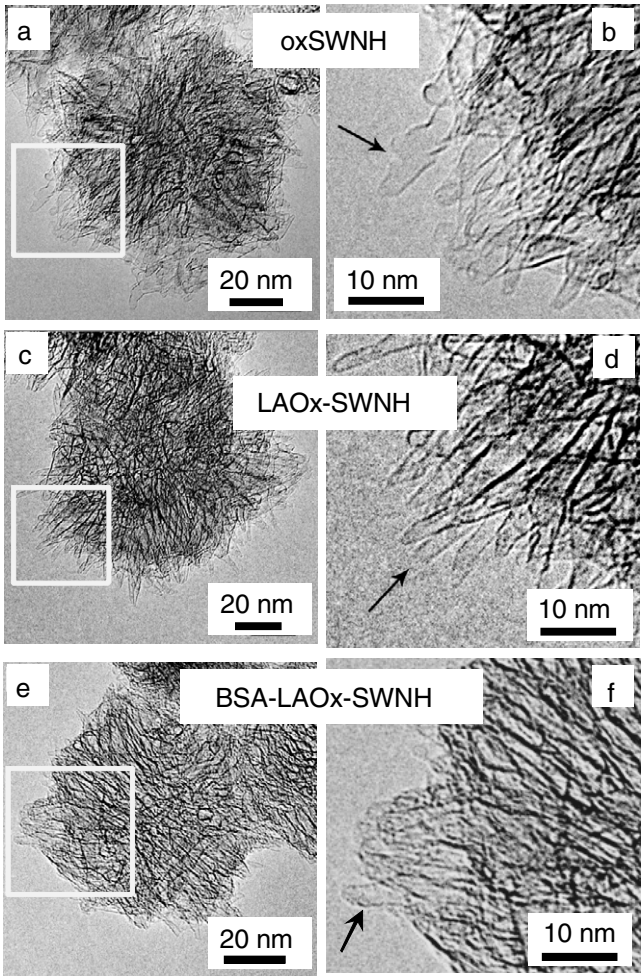


**Figure 2.** TEM images of oxSWNH ((a) and (b)), LAOx-SWNH ((c) and (d)), and BSA–LAOx-SWNH ((e) and (f)) agglomerates. The arrows indicate holes ((b) and (d)) and BSA moieties (f).

The pore volumes of oxSWNH (0.92 ml $g^{-1}$) and LAOx-SWNH (0.68 ml $g^{-1}$) were larger than those of as-grown SWNHs (0.42 ml $g^{-1}$; table 1, supporting information I and III (available at stacks.iop.org/Nano/22/265106/mmedia). See also section 2), indicating that their holes were open. The pore volume of BSA–LAOx-SWNH was similar to that of as-grown SWNHs, indicating that BSA molecules were attached to the hole edges [17] and blocked the holes (table 1).

Dispersion of the specimens in PBS was first examined by sight (figures 3(a), (c) and (e)). The sonically dispersed oxSWNHs and LAOx-SWNHs settled down considerably after 5 min and 60 min, respectively (figures 3(a) and (c)), but BSA–LAOx-SWNHs maintained the almost-homogeneous dispersion, even after a day or more (figure 3(e)) [18]. Corresponding to these dispersion states, the particle size measured by DLS was large for oxSWNHs (sub-micrometers to micrometers) and LAOx-SWNHs (sub-micrometers) but small for BSA–LAOx-SWNHs (approximately 120 nm; figures 3(b), (d) and (f), table 1). These results suggest that oxSWNH aggregates and LAOx-SWNH aggregates were agglomerated in PBS, while BSA–LAOx-SWNH aggregates almost individually dispersed. These dispersion differences

**Table 1.** Physicochemical data of oxSWNH, LAOx-SWNH and BSA–LAOx-SWNH. Note: [ ]: method, oxy: oxygenated groups.

| | Dispersion in PBS [by site] | Particle size in PBS [DLS] | Functional groups (%) | $\zeta$ potential in PBS (mV) | Pore volume (ml $g^{-1}$) |
|---|---|---|---|---|---|
| oxSWNH | Unstable | Sub-micrometer–micrometer | Oxy: 1–2 | −37 | 0.92 |
| LAOx-SWNH | Unstable | Sub-micrometer | Oxy: ∼20 | −37 | 0.68 |
| BSA–LAOx-SWNH | Stable | ∼120 nm | Oxy: ∼20, BSA: ∼14 | −36 | 0.42[a] |

[a] This value coincides with the pore volume of as-grown SWNHs, 0.42 ml $g^{-1}$ [19].

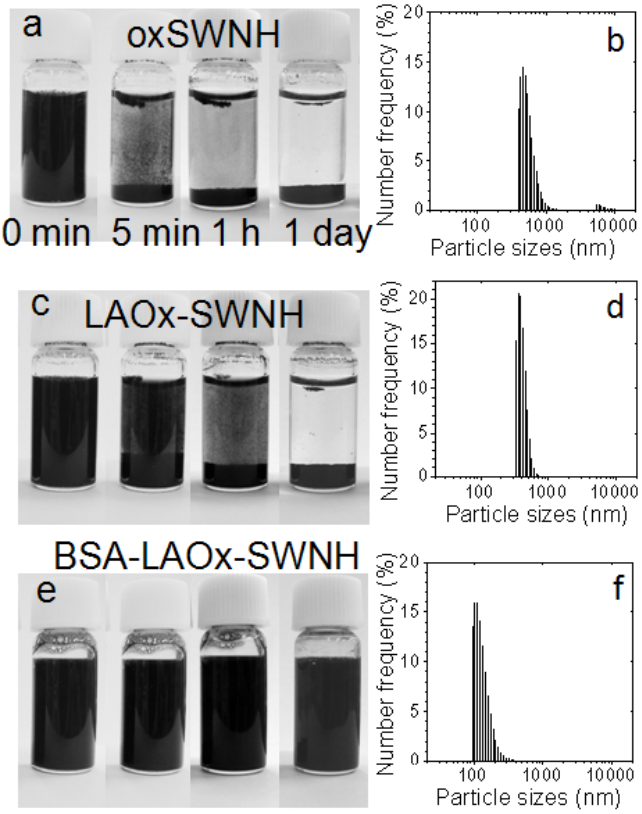


**Figure 3.** Images of dispersions of oxSWNHs (a), LAOx-SWNHs (c) and BSA–LAOx-SWNHs (e) in PBS. From left to right: immediately after sonication, 5 min, 60 min and 1 day. Particle size distributions for oxSWNHs (b), LAOx-SWNHs (d) and BSA–LAOx-SWNHs (f).

were correlated with the number of hydrophilic groups. The quantity of oxygenated groups estimated from TGA in $O_2$ was small in oxSWNH (1–2%) and large in LAOx-SWNH and BSA–LAOx-SWNH (∼20%). Furthermore, BSA–LAOx-SWNH had additional BSA moieties (∼14%; table 1, supporting information II available at stacks.iop.org/Nano/22/265106/mmedia). The degree of dispersion of the specimens did not have any correlation with $\zeta$ potential or the pore volume (table 1).

### 3.2. Animal tests

*3.2.1. Toxicological assessments.* All animals survived all the test periods after single-dose intravenous administration of nanohorn dispersion in PBS. No statistically significant differences were observed in body weight between the groups treated with the vehicle, oxSWNHs, LAOx-SWNHs and BSA–LAOx-SWNHs (supporting information IV available at stacks.iop.org/Nano/22/265106/mmedia). No clinical symptoms or signs of abnormalities were observed for any animals on gross observation (supporting information V available at stacks.iop.org/Nano/22/265106/mmedia).

Histopathological observation revealed that black particles of oxSWNHs, LAOx-SWNHs or BSA–LAOx-SWNHs were present in the lungs, liver and spleen of all SWNH-treated animals. Vessel wall thickening (yellow paste in supporting information VI and VII available at stacks.iop.org/Nano/22/265106/mmedia) caused by large agglomerates of oxSWNHs occupying the vessel lumens were found at 2 w in the lungs. Vessel wall thickening was alleviated when the agglomerate size reduced during the later periods (supporting information VI and VII available at stacks.iop.org/Nano/22/265106/mmedia). Abnormal cellular degeneration/necrosis was not observed (supporting information VI available at stacks.iop.org/Nano/22/265106/mmedia), which may suggest that oxSWNH, LAOx-SWNH and BSA–LAOx-SWNH do not potentially cause severe tissue damage. The black agglomerates of oxSWNHs, LAOx-SWNHs and BSA–LAOx-SWNHs were not found in the kidneys, heart and brain, since no toxicological signs were obvious on histological observation.

*3.2.2. Biodistribution.* The number and size of black particles of oxSWNHs, LAOx-SWNHs and BSA–LAOx-SWNHs found in the lungs, liver and spleen at 2 w and 26 w are presented in table 2. The details of the number of black particles are shown in the shadowed lines in supporting information VI (available at stacks.iop.org/Nano/22/265106/mmedia). In table 2, the number of black agglomerates of nanohorns observed under an optical microscope (100× magnification, visible agglomerate sizes >5 $\mu$m) are indicated with a '+'. The largest size of black agglomerates is also indicated in table 2. Figure 4 shows the 'maximum size' and 'average number of + symbols' indicated in table 2. The 'maximum size' in the spleen is shown only for the zones (red pulp, white pulp or marginal zones), where the nanohorn number was the highest.

*OxSWNH.* The highly hydrophobic oxSWNHs mainly accumulated in the lungs and hardly in the liver and spleen (table 2, figure 4). The hydrophobic property induced many oxSWNHs to form large agglomerates, reaching 50 $\mu$m in the lungs at 2 w, but their number and size decreased at 26 w (table 2, figures 4, 5(a) and (b)). In addition to the large

**Table 2.** The number and size of agglomerates found in the tissue sections on optical microscopy. +: score for the number of black agglomerates of SWNHs observed at 100×. Numbers to the right of '+' indicate the number of mice. The size is shown with maximum agglomerate sizes. (Note: +: score for the number of black agglomerates of SWNHs observed at 100×. <+: less than '+'. *n*: number of mice.)

| | oxSWNH | | | | LAOx-SWNH | | | | BSA–LAOx-SWNH | | | |
|---|---|---|---|---|---|---|---|---|---|---|---|---|
| | 2 w | | 26 w | | 2 w | | 26 w | | 2 w | | 26 w | |
| | Size ($\mu$m) | Score, *n* | Size ($\mu$m) | Score, *n* | Size ($\mu$m) | Score, *n* | Size ($\mu$m) | Score, *n* | Size ($\mu$m) | Score, *n* | Size ($\mu$m) | Score, *n* |
| Lung | <60* | ++ 0 | <30 | ++ 2 | <7 | ++ 3 | <15 | ++ 0 | <20 | ++ 0 | <30 | ++ 0 |
| | | +++ 3 | | +++ 3 | | +++ 2 | | +++ 5 | | +++ 5 | | +++ 5 |
| | | ++++ 2 | | ++++ 0 | | ++++ 0 | | ++++ 0 | | ++++ 0 | | 0 |
| Liver | <2 | <+ 4 | <5 | <+ 4 | <5 | <+ 3 | <10 | <+ 0 | <3 | <+ 5 | <5 | <+ 4 |
| | | + 1 | | + 1 | | + 2 | | + 3 | | + 0 | | + 1 |
| | | ++ 0 | | ++ 0 | | ++ 0 | | ++ 2 | | ++ 0 | | ++ 0 |
| Spleen | | | | | | | | | | | | |
| Marginal zone | <3 | | | <+ 4 | <5 | | | <+ 5 | <3 | | | <+ 5 |
| | | + 5 | | + 1 | | + 0 | | + 0 | | + 5 | | + 0 |
| | | ++ 0 | | ++ 0 | | ++ 5 | | | | ++ 0 | | |
| Red pulp | | <+ 5 | | <+ 3 | | <+ 2 | | <+ 0 | | <+ 4 | | <+ 4 |
| | | + 0 | | + 2 | | + 3 | | + 5 | | + 1 | | + 1 |
| White pulp | | <+ 5 | <5 | | | <+ 5 | <10 | | | <+ 5 | <4 | |
| | | + 0 | | + 5 | | + 0 | | + 0 | | + 0 | | + 4 |
| | | ++ 0 | | ++ 0 | | ++ 0 | | ++ 3 | | ++ 0 | | ++ 1 |
| | | | | | | | | + + + 2 | | | | |

agglomerates, archipelago-like assemblies of small oxSWNH agglomerates existed in the interstitium, which did not change with time (figures 5(c) and (d)).

In the liver and spleen, the size (several micrometers) and number of oxSWNH agglomerates were much smaller (figures 5(e), (f), (i) and (j)) than those in the lungs, which did not change considerably throughout the test periods (table 2, figure 4).

In the spleen, the intra-organ movement of oxSWNH agglomerates from the marginal zone at 2 w (figures 5(g), (i) and table 2) to the white pulp, often near the central arteries (figures 5(h), (j) and table 2), at 26 w was apparent.

*LAOx-SWNH.* Because LAOx-SWNHs are slightly more hydrophilic, their biodistribution was different compared to that of oxSWNHs. LAOx-SWNHs were distributed rather evenly in the lungs, liver and spleen, and their size and number increased with time (table 2 and figure 4). In the lungs, liver and spleen, the small agglomerates (<5 $\mu$m) often arranged separately or formed an 'archipelago' (figures 6(a), (c) and (g)) at 2 w, which gathered and formed dense and/or large (sometimes with overall sizes of 10 $\mu$m) 'archipelagoes' at 26 w (figures 6(b), (d), (h) and (j)). Most of the agglomerates in the lungs were found in the interstitium (figures 6(a) and (b)).

The intra-spleen movement of LAOx-SWNHs from the marginal zone (figures 6(e) and (g)) to the white (figures 6(f) and (h)) and red pulps (figures 6(i) and (j)) were also apparent (table 2).

*BSA–LAOx-SWNH.* Although BSA–LAOx-SWNHs are highly hydrophilic, their biodistribution pattern was between those of the slightly hydrophilic LAOx-SWNH and the hydrophobic oxSWNH as shown in figures 4 and 7.

In the spleen, movement of BSA–LAOx-SWNHs was slightly different from the other two nanohorns. The movement from marginal zones (2 w; figures 7(e) and (g)) to the white pulps (26 w; figures 7(f) and (h)) was obvious, but movement to the red pulps was not clear (table 2).

## 4. Discussion

### *4.1. Intravenous toxicities*

No histological abnormalities such as granuloma or fibrosis, potential pathological lesions caused by rigid and long MWNTs, were observed, suggesting that nanohorns cannot be highly pathogenic. This is probably because the nanohorn aggregate has a small size of approximately 100 nm and are bound to each other by weak van der Waals forces, resulting in easy separation of the individual agglomerates.

In the spleen, the nanohorn species existed around the central artery where T cells usually exist (figures 5–7). The absence of undesired inflammatory responses suggests that macrophages could not digest the robust nanohorns, and no signal was presented at the macrophages. The uptake of nanohorns by macrophages, stained brown with CD107b, were observed as shown in figures 8(a)–(c) for LAOx-SWNHs.

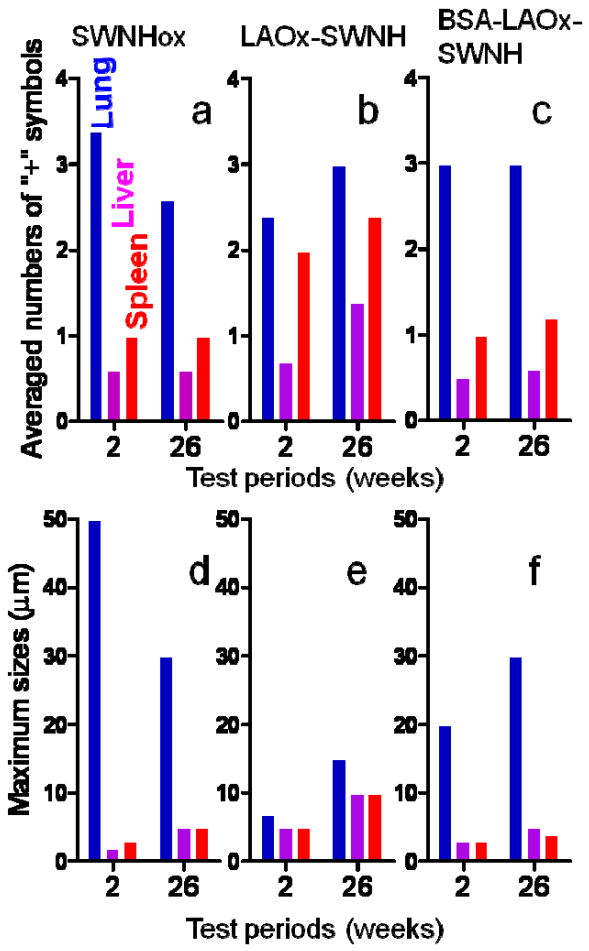


**Figure 4.** Average number of '+' symbols in table 2 for oxSWNHs (a), LAOx-SWNHs (b) and BSA–LAOx-SWNHs (c), which correspond to agglomerate number. Maximum size of agglomerates in table 2 for oxSWNHs (d), LAOx-SWNH (e) and BSA–LAOx-SWNH (f). Color codes: blue (lung), magenta (liver) and red (spleen).

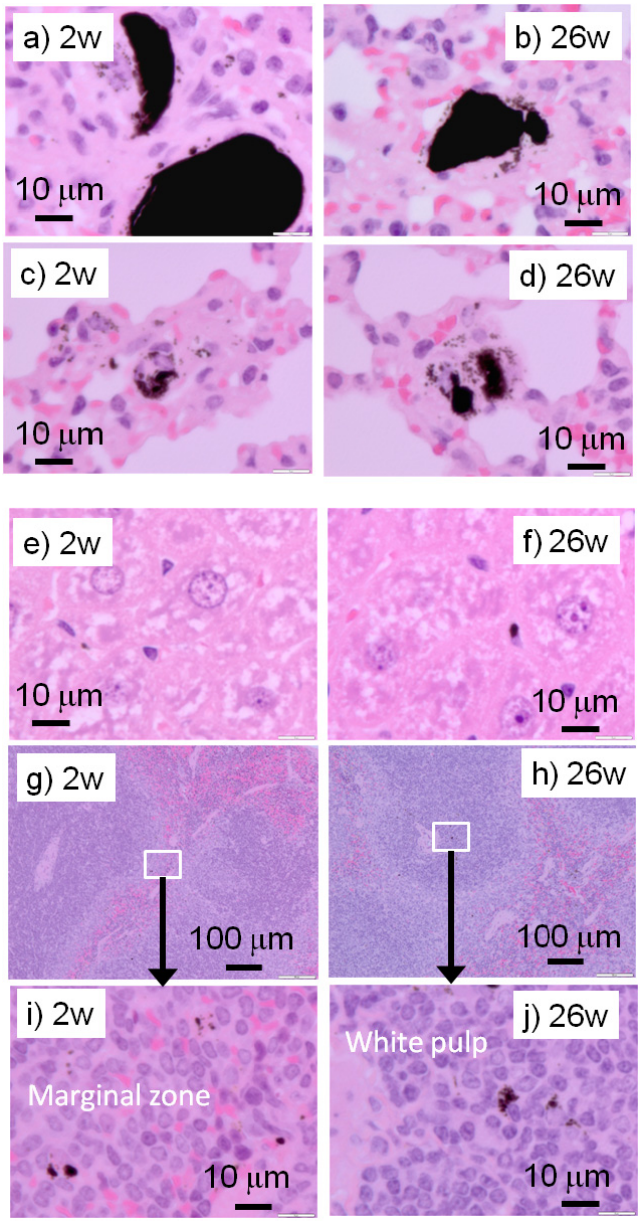


**Figure 5.** Optical microscope images of tissues from the lungs ((a) and (d)), liver ((e) and (f)), and spleen ((g) and (j)) of mice anatomized at 2 (left) and 26 weeks (right) after single-dose intravenous administration of oxSWNHs. (HE staining).

### *4.2. Biodistribution of nanohorns was influenced by functionalization*

The nanohorn biodistribution and its changes with time depend on the functionalizations of nanohorns, perhaps because the interaction of macrophages with nanohorns depends on the functionalized moieties. Both LAOx-SWNH and BSA–LAOx-SWNH tended to increase the agglomerate number, size and density with time in the lungs, liver and spleen (table 2, figures 4, 6 and 7). These changes may be attributed to the macrophages' engulfing/collecting small agglomerates as inferred from the CD107b brown-stained macrophages interacting with nanohorn agglomerates (figure 8(e)). The effect of BSA was apparent in the agglomeration of BSA–LAOx-SWNHs in the lungs, which was larger than that of LAOx-SWNHs (figure 4(f)). This tendency contradicts the results in PBS, in which BSA–LAOx-SWNH has a smaller agglomerate size than LAOx-SWNH (figure 3). We believe that the BSA moieties stimulated the macrophages and enhanced their uptake of nanohorns in the lungs, resulting in higher accumulation. The macrophage uptake enhancement of LAOx-SWNH by the BSA attachment has been confirmed *in vitro* (data not shown). The BSA moieties also influenced the movement of BSA–LAOx-SWNH in the spleen, though its mechanism is unclear.

OxSWNHs, which are different from LAOx-SWNHs and BSA–LAOx-SWNHs, form extremely large agglomerates due to their highly hydrophobic properties, thus occupying the lung vessel lumens (figure 5). The agglomerate size of oxSWNHs in the lungs decreased from 2 w to 26 w (table 2 and figure 4), perhaps because the large oxSWNH agglomerates separated into small pieces in the bloodstream. These small pieces may be captured by macrophages (figure 8(d)); however, the capture was not particularly effective and, as a result, both the number and size of oxSWNH agglomerates in the lungs decreased from

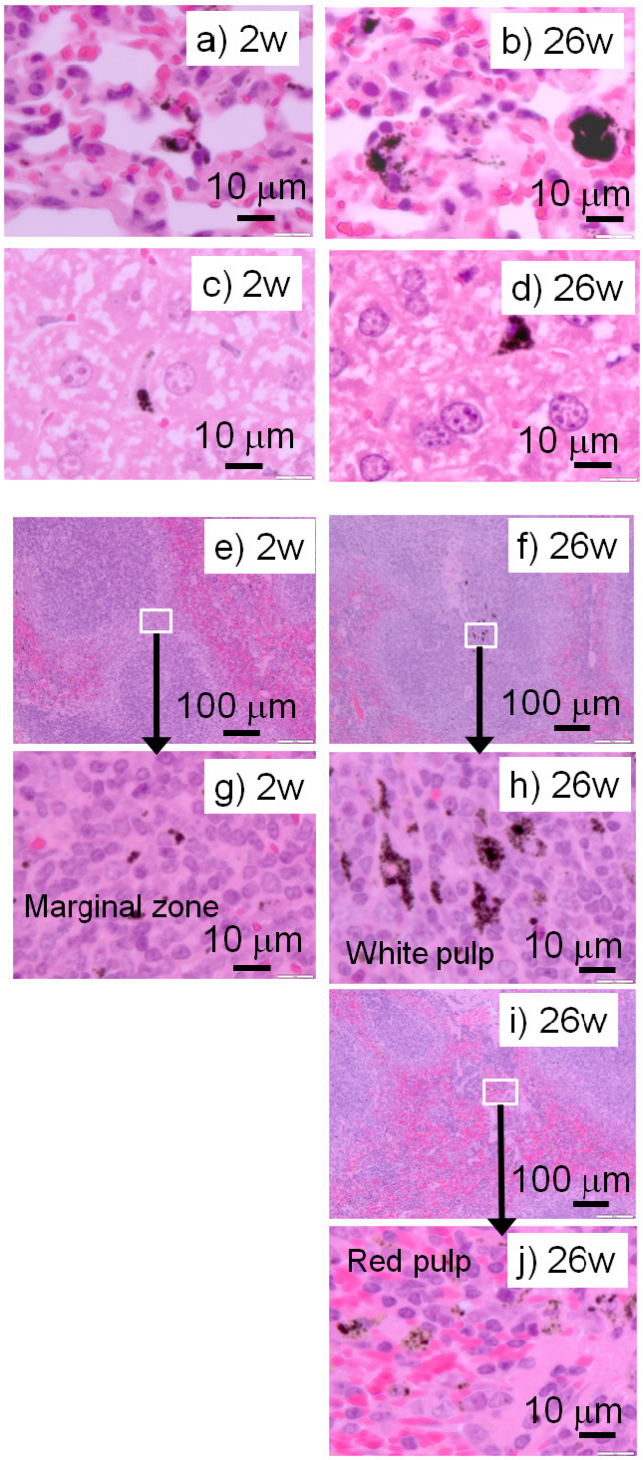


**Figure 6.** Optical microscope images of tissues from the lungs ((a) and (b)), liver ((c) and (d)), and spleen ((e)–(j)) of mice anatomized at 2 (left) and 26 weeks (right) after single-dose intravenous administration of LAOx-SWNH (HE staining).

2 w to 26 w (figure 4(a) and table 2). This suggests that a certain amount of oxSWNHs was cleared from the lungs. The movement of oxSWNHs from the lungs to the liver or spleen was not the main reason for the clearance from the lungs because the size and number of oxSWNHs in the liver and spleen did not increase considerably (figures 4(a), (d) and

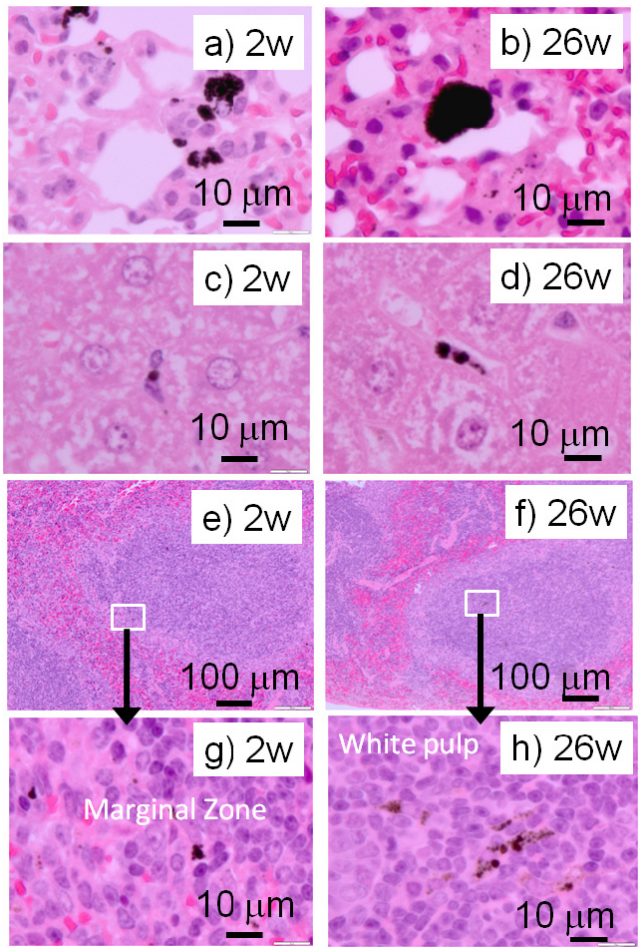


**Figure 7.** Optical microscope images of tissues from the lungs ((a) and (b)), liver ((c) and (d)), and spleen ((e)–(h)) of mice anatomized at 2 (left) and 26 weeks (right) after single-dose intravenous administration of BSA–LAOx-SWNHs (HE staining).

table 2). A certain amount of oxSWNHs may be excreted to the airways through the lung alveoli with the support of macrophages, though no evidence is available, and to our knowledge no such phenomenon has been reported.

## 5. Summary

The functionalized nanohorns, intravenously injected in the tails of mice, accumulated primarily in the lungs, liver and spleen, but little accumulation was observed in the heart, kidneys and brain. OxSWNHs, LAOx-SWNHs and BSA–LAOx-SWNHs did not show high toxicity, confirmed by the normal gross appearance and normal weight gain of the mice. No severe abnormalities in the tissues were found on histological observations.

The biodistribution of nanohorns was significantly influenced by chemical functionalization. Highly hydrophobic oxSWNHs formed large agglomerates and accumulated primarily in the lungs. LAOx-SWNHs with slightly higher hydrophilicity distributed nearly evenly in the lungs, liver and spleen. Although BSA–LAOx-SWNHs were highly hydrophilic, due to the BSA moieties, they were mostly captured by the macrophages, and accumulated in the lungs.

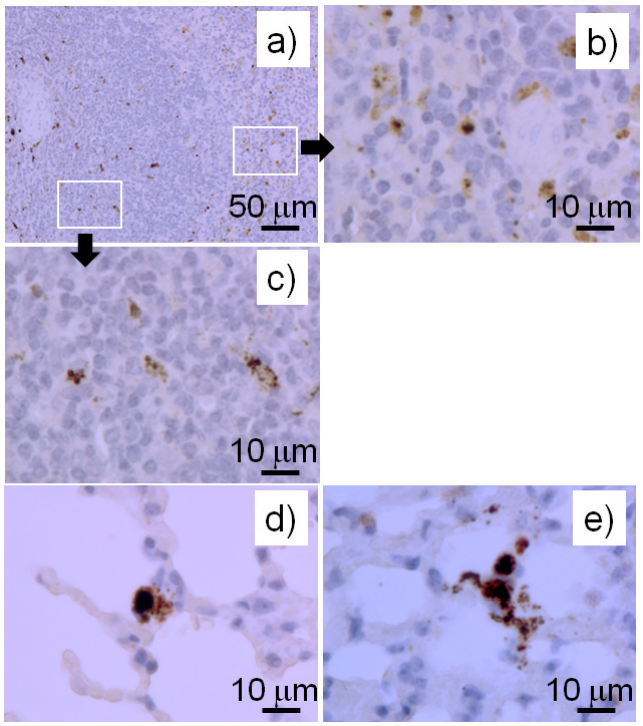


**Figure 8.** Immunohistochemical detection of macrophages in spleen of mice anatomized at 26 weeks ((a)–(c)) after single-dose intravenous administration of LAOx-SWNHs and in lungs of mice anatomized at 26 weeks after single-dose intravenous administration of oxSWNHs (d) and BSA–LAOx-SWNHs (e).

The time course of the biodistribution and agglomeration structure was observed, which would be caused by the action of the macrophages. The agglomerate size increased with time, probably because macrophages engulfed and collected the nanohorn agglomerates. The exceptional case was oxSWNH in the lungs. The extremely large agglomerates of oxSWNHs, as large as 50 $\mu$m in the lungs, decreased in size with time, probably because they separated into small pieces that were collected by macrophages.

In the spleen, the macrophages could carry the nanohorns from marginal zones to the red and white pulps. In the white pulps, nanohorn-laden macrophages aggregated around the central artery typically populated by many T cells. However, no immunological lesions were histologically observed, perhaps because the chemically stable nanohorns cannot generate chemical species that enable the signal expression at the macrophage surface.

## Acknowledgments

We thank Dr T Azami and Dr D Kasuya (NEC Co.) for preparing SWNHs and Ms F Jing (JST/SORST) for the TEM observation. We also thank Toray Research Center, Inc. for experimental support and discussions.

## References

[1] Iijima S 1991 Helical microtubules of graphitic carbon *Nature* **354** 56–8

[2] Kroto H W, Heath J R, O'Brien S C, Curl R F and Smalley R E 1985 $C_{60}$: Buckminsterfullerene *Nature* **318** 162–3

[3] Scheinberg D A, Villa C H, Escorcis F E and McDevitt M R 2010 Conscripts of the infinite armada: systematic cancer therapy using nanomaterials *Nat. Rev. Clin. Oncol.* **7** 266–76

[4] Lacerda L, Bianco A, Prato M and Kostarelos K 2006 Carbon nanotubes as nanomedicines: from toxicology to pharmacology *Adv. Drug Deliv. Rev.* **58** 1460–70

[5] Liu Z, Sun X, Nakayama-Ratchford N and Dai H 2007 Supramolecular chemistry on water-soluble carbon nanotubes for drug loading and delivery *ACS Nano* **1** 50–6

[6] Nielsen G D, Roursgaard M, Jensen K A, Poulsen S S and Larsen S T 2008 *In vivo* biology and toxicology of fullerenes and their derivatives *Basic Clin. Pharmacol. Toxicol.* **103** 197–208

[7] Takagi A, Hirose A, Nishimura T, Fukumori N, Ogata A, Ohashi N, Kitajima S and Kanno J 2008 Induction of mesothelioma in p53 + /− mouse by intraperitoneal application of multi-wall carbon nanotube *J. Toxicol. Sci.* **33** 105–16

[8] Kokosnjaj-Tabi J, Hartman K B, Boudjemaa S, Ananta J S, Morgant G, Szwarc H, Wilson L and Moussa F 2010 *In vivo* behavior of large doses of ultrashort and full-length single-walled carbon nanotubes after oral and intraperitoneal administration to Swiss mice *ACS Nano* **4** 1481–92

[9] Wick P, Manser P, Limbach L K, Dettlaff-Weglikowska U, Krumeich F, Roth S, Stark W J and Bruinink A 2007 The degree and kind of agglomeration affect carbon nanotube cytotoxicity *Toxicol. Lett.* **168** 121–31

[10] Kostarelos K 2008 The long and short carbon nanotube toxicity *Nat. Biotechnol.* **26** 774–6

[11] Poland C A, Duffin R, Kinloch I, Maynard A, Wallace W A, Seaton A, Stone V, Brown S, MacNee W and Donaldson K 2008 Carbon nanotubes introduced into the abdominal cavity of mice show asbestos-like pathogenicity in a pilot study *Nat. Nanotechnol.* **3** 423–8

[12] Riviere J E 2008 Pharmacokinetics of nanomaterials: an overview of carbon nanotubes, fullerenes and quantum dots *Wiley Interdiscip. Rev. Nanomed. Nanobiotechnol.* **1** 26–34

[13] Lacerda L, Herrero M A, Venner K, Bianco A, Prato M and Kostarelos K 2008 Carbon-nanotube shape and individualization critical for renal excretion *Small* **4** 1130–2

[14] Liu Z, Davis C, Cai W, He L, Chen X and Dai H 2008 Circulation and long-term fate of functionalized, biocompatible single-walled carbon nanotubes in mice probed by Raman spectroscopy *Proc. Natl Acad. Sci. USA* **105** 1410–5

[15] Iijima S, Yudasaka M, Yamada R, Bandow S, Suenaga K, Kokai F and Takahashi K 1999 Nano-aggregates of single-walled graphitic carbon nano-horns *Chem. Phys. Lett.* **309** 165–70

[16] Miyawaki J, Yudasaka M, Azami T, Kubo Y and Iijima S 2008 Toxicity of single-walled carbon nanohorns *ACS Nano* **2** 213–26

[17] Fan J, Yudasaka M, Miyawaki J, Ajima K, Murata K and Iijima S 2006 Control of hole opening in single-wall carbon nanotubes and single-wall carbon nanohorns using oxygen *J. Phys. Chem.* B **110** 1587–91

[18] Zhang M, Yudasaka M, Ajima K, Miyawaki J and Iijima S 2007 Light-assisted oxidation of single-wall carbon nanohorns for abundant creation of oxygenated groups that enable chemical modifications with proteins to enhance biocompatibility *ACS Nano* **1** 265–72

[19] Yudasaka M, Fan J, Miyawaki J and Iijima S 2005 Studies on the adsorption of organic materials inside thick carbon nanotubes *J. Phys. Chem.* B **109** 8909–13